Influence of strain on thermal conductivity of silicon nitride thin films



2012 J. Micromech. Microeng. 22 045001

(http://iopscience.iop.org/0960-1317/22/4/045001)

# Report Documentation Page

*Form Approved*
*OMB No. 0704-0188*



| 1. REPORT DATE | 2. REPORT TYPE | 3. DATES COVERED |
|---|---|---|
| **MAR 2012** | | **00-00-2012 to 00-00-2012** |

| 4. TITLE AND SUBTITLE | 5a. CONTRACT NUMBER |
|---|---|
| **Influence Of Strain On Thermal Conductivity Of Silicon Nitride Thin Films** | 5b. GRANT NUMBER |
| | 5c. PROGRAM ELEMENT NUMBER |
| 6. AUTHOR(S) | 5d. PROJECT NUMBER |
| | 5e. TASK NUMBER |
| | 5f. WORK UNIT NUMBER |
| 7. PERFORMING ORGANIZATION NAME(S) AND ADDRESS(ES) **Air Force Research Laboratory,Thermal Sciences and Materials Branch,Wright-Patterson Air Force Base,OH,45433** | 8. PERFORMING ORGANIZATION REPORT NUMBER |
| 9. SPONSORING/MONITORING AGENCY NAME(S) AND ADDRESS(ES) | 10. SPONSOR/MONITOR'S ACRONYM(S) |
| | 11. SPONSOR/MONITOR'S REPORT NUMBER(S) |

12. DISTRIBUTION/AVAILABILITY STATEMENT
**Approved for public release; distribution unlimited**

13. SUPPLEMENTARY NOTES
**Journal Of Micromechanics And Microengineering, 2 March 2012**

14. ABSTRACT
**We present a micro-electro-mechanical system-based experimental technique to measure thermal conductivity of freestanding ultra-thin films of amorphous silicon nitride (Si3N4) as a function of mechanical strain. Using a combination of infrared thermal micrography and multi-physics simulation, we measured thermal conductivity of 50 nm thick silicon nitride films to observe it decrease from 2.7 W (m K)−1 at zero strain to 0.34 W (m K)−1 at about 2.4% tensile strain. We propose that such strain?thermal conductivity coupling is due to strain effects on fraction?phonon interaction that decreases the dominant hopping mode conduction in the amorphous silicon nitride specimens.**

15. SUBJECT TERMS

| 16. SECURITY CLASSIFICATION OF: | | | 17. LIMITATION OF ABSTRACT | 18. NUMBER OF PAGES | 19a. NAME OF RESPONSIBLE PERSON |
|---|---|---|---|---|---|
| a. REPORT **unclassified** | b. ABSTRACT **unclassified** | c. THIS PAGE **unclassified** | **Same as Report (SAR)** | **10** | |

J. Micromech. Microeng. **22** (2012) 045001 (8pp) doi:10.1088/0960-1317/22/4/045001

# Influence of strain on thermal conductivity of silicon nitride thin films

**M T Alam[1], M P Manoharan[1], M A Haque[1,3], C Muratore[2] and A Voevodin[2]**

[1] Department of Mechanical and Nuclear Engineering, Penn State University, University Park, PA 16802, USA
[2] Air Force Research Laboratory, Thermal Sciences and Materials Branch, Wright-Patterson Air Force Base, OH 45433, USA

E-mail: mah37@psu.edu

Received 20 October 2011, in final form 20 January 2012
Published 2 March 2012
Online at stacks.iop.org/JMM/22/045001

**Abstract**
We present a micro-electro-mechanical system-based experimental technique to measure thermal conductivity of freestanding ultra-thin films of amorphous silicon nitride ($Si_3N_4$) as a function of mechanical strain. Using a combination of infrared thermal micrography and multi-physics simulation, we measured thermal conductivity of 50 nm thick silicon nitride films to observe it decrease from 2.7 W (m K)$^{-1}$ at zero strain to 0.34 W (m K)$^{-1}$ at about 2.4% tensile strain. We propose that such strong strain–thermal conductivity coupling is due to strain effects on fraction–phonon interaction that decreases the dominant hopping mode conduction in the amorphous silicon nitride specimens.

(Some figures may appear in colour only in the online journal)

## 1. Introduction

Multi-domain (electrical, mechanical and thermal, to name a few) coupling is an essential feature of micro- and nanoscale devices and systems [1]. The same is true for other applications in micro-electronics [2, 3], opto-electronics [4, 5], flexible electronics [6, 7] and energy conversion [8, 9]. These devices are commonly fabricated out of thin film materials, which experience mechanical strain during deposition as well as device operation. Mechanical reliability of thin films is therefore as important as their transport (electrical and thermal) properties. While electro-mechanical coupling is commonly exploited in microelectronic and other small-scale systems, the thermal domain must also be considered in these applications, whether due to intentional design or unintentional coupling (for example, excessive heat generation in chips [10]). Thermo-mechanical coupling in thin films is typically studied in terms of temperature effects on mechanical properties [11–13] and not from a thermal transport perspective. The fundamental question whether mechanical strain can influence thermal transport is therefore the core theme for this study.

In this paper, we investigate low pressure chemical vapor deposited silicon nitride (LPCVD $Si_3N_4$) thin films. Silicon nitride is prevalently used for isolation, passivation, etch masking as well as structural and optical layers for various micro-electronic, opto-electronic and micro-electro-mechanical systems [14–17]. It also experiences very large residual strain during deposition and exerts similar strains to other thin film materials attached to it, which makes it a suitable candidate for this study. In fact, the large elastic strain has led researchers to propose silicon nitride substrates to tune the electron mobility in microelectronic devices [18, 19]. Further motivation for this study comes from the observation that the role of mechanical deformation on thermal conductivity has been computationally explored by only a few researchers [20–24] and experimental efforts have appeared in the literature only very recently [25–27].

A brief review of the state of the art in thermal conductivity of silicon nitride is given below. Mastrangelo *et al* [28] measured thermal conductivity of microns thick silicon nitride films to be around 3.2 W (m K)$^{-1}$. Zhang and Grigoropuolos [29] observed anomalous thickness dependence and suggested that microstructural defects may strongly influence thermal conductivity. Jain and Goodson [30] measured the in-plane

[3] Author to whom any correspondence should be addressed.

 

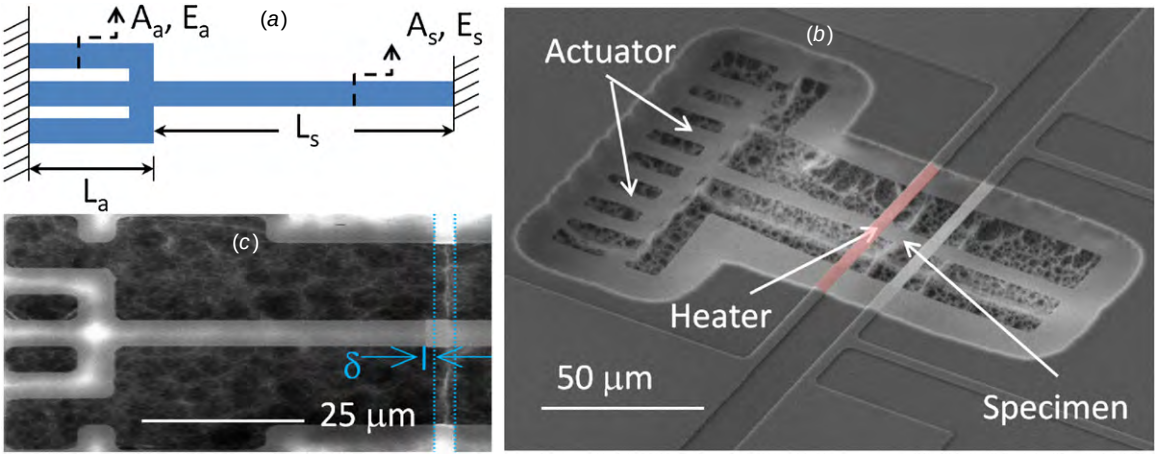


**Figure 1.** (*a*) Schematic diagram showing a single layer silicon nitride three-strip actuator and a specimen. (*b*) Scanning electron micrograph of a specimen integrated with a five-strip actuator and a thin film heater. (*c*) Strain is measured after post-experiment fracture of the specimen.

thermal conductivity of 1.5 $\mu$m thick specimens to be about 5 W (m K)$^{-1}$. At the nanoscale, Sultan *et al* [31] reported thermal conductivity of 500 nm thin films as 3–4 W (m K)$^{-1}$ for a temperature range of 77–325 K. For 180–220 nm thick low stress nitride, Zink and Hellman [32] observed stronger temperature effects thermal conductivity varying from 0.07 to 4 W (m K)$^{-1}$ at a temperature range of 3–300 K. The cross-plane thermal conductivity measured by Lee and Cahill [33] and Shin *et al* [34] for less than 100 nm thickness was in the range of 0.4–0.7 W (m K)$^{-1}$, showing very strong pseudo-size effects, which were ascribed to the interfacial thermal resistance. Stojanovich *et al* [35] measured thermal conductivity of 180 nm thick freestanding specimens to be about 2.1 W (m K)$^{-1}$. Bai *et al* [36] measured thermal conductivity of stoichiometric silicon nitride to be about 1.2–2.0 W (m K)$^{-1}$ for thicknesses of 37–200 nm thick films. It is very important to note that none of the above studies measure thermal conductivity as a function of mechanical strain. Even though the specimens are typically freestanding, the mechanical boundary conditions result in about 0.2%–0.3% residual strain depending on the silicon-to-nitrogen ratio.

## 2. Device design and fabrication

Silicon nitride is a very brittle material with unusually large tensile residual stress, which makes its thermo-physical characterization challenging. Common approaches are to synthesize low stress, silicon rich ($SiN_x$, $x = 1$–1.1) nitride or to study the specimen on a rigid substrate. Because the interfacial thermal resistance is challenging to measure and plays a significant role in nanoscale experiments, studies on freestanding specimens are desirable. Characterization and control of the amount of stress or strain in ultra-thin specimens are also challenging. To obtain specimens with different values of strain, one needs to vary the deposition parameters from wafer to wafer, which is cumbersome and also changes the composition and microstructure of the specimen. We address this issue with the concept of 'self-actuation' by exploiting the tensile residual stress in silicon nitride. Here, we design both actuator and the specimen in the same film plane but increase the cross-sectional area of the actuator portion compared to the specimen. This is shown in figure 1(*a*), where three actuator strips are patterned in series with the specimen. Before their release from the substrate, both actuator and specimen experience the same tensile strain (residual strain after deposition). However, removal of the substrate also removes the uniform strain level and force distribution in the freestanding actuator and specimen, which is re-organized according to their respective cross-sectional areas. Because of its larger cross-sectional area, the three actuator strips (with the length $L_a$ and cross-sectional area $A_a$) will apply a tensile force on the specimen (with the length $L_s$ and cross-sectional area $A_s$). The amount of this force and associated strain can be controlled by the actuator design utilizing the force equilibrium condition

$$F = k_a\delta_a = k_s\delta_s, \tag{1}$$

where $k$ is stiffness, $\delta$ is the net displacement and the subscripts $a$ and $s$ denote the actuator and specimen, respectively. The equilibrium equation can thus be written as a function of the length ($L$), cross-sectional area ($A$) and Young's modulus ($E$) of the actuator and specimen

$$n\frac{E_aA_a}{L_a}\delta_a = \frac{E_sA_s}{L_s}\delta_s, \tag{2}$$

where $n$ is the number of actuator strips. Larger value of $n$ implies higher value of stress and strain on the specimen. However, experimental results deviate more than 25% from the model for $n > 5$ because of the compliance of the outer actuator strips compared to the inner ones. We note that the total displacement in the fabricated structure, $\delta$, is the sum of the actuator and specimen displacement ($\delta_a + \delta_s = \delta$). This displacement can be measured by fracturing the specimen after the experiment and then measuring the gap between the fractured surfaces. Therefore, irrespective of the overestimation (if at all) of the model, the resolution of strain measurement is governed by the scanning electron microscope magnification. Using the force equilibrium equation, we can

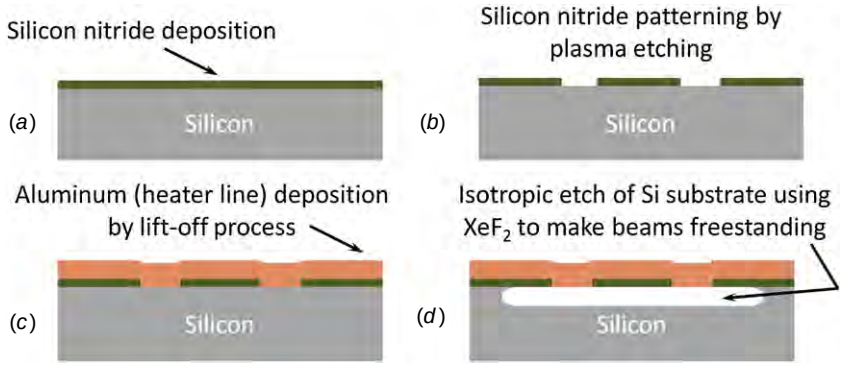


**Figure 2.** Fabrication processing for the device integrating the actuator, specimen and heater for thermal conductivity characterization.

relate the specimen displacement with the total displacement as follows:

$$\delta_s \left[1 + \frac{E_s A_s L_a}{n E_a A_a L_s}\right] = \delta. \tag{3}$$

The strain in the specimen, $\varepsilon_s$, is then given by

$$\varepsilon_s = \frac{\delta_s}{L_s} = \frac{\delta n E_a A_a}{(n E_a A_a L_s + E_s A_s L_a)}. \tag{4}$$

For this study, the actuator and the specimen are fabricated from the same material. The specimen strain is therefore given by

$$\varepsilon_s = \frac{\delta n A_a}{(n A_a L_s + A_s L_a)}. \tag{5}$$

The device fabrication process is schematically described in figure 2. The process starts with a deposition of 50 nm thick freestanding LPCVD $Si_3N_4$ using ammonia and dichlorosilane at 820 °C (figure 2(*a*)). The residual stress in the deposited film is about 1.2 GPa. The device design shown in figure 1(*a*) is then patterned on the nitride layer using lithography, after which the exposed nitride is etched with reactive ion etching using $CF_4/O_2$ plasma. This is shown in figure 2(*b*). Using the front side alignment, negative lithography is performed to pattern a line perpendicular to the silicon nitride line and 175 nm thick aluminum film is evaporated to complete the lift-off process. Figure 1(*c*) shows the aluminum and nitride lines patterned on the silicon wafer, which are still attached to the substrate. The next step is to release the two lines using isotropic $XeF_2$ etching. Figure 2(*d*) shows the freestanding nitride specimen and the aluminum heater line schematically, for which a scanning electron micrograph is shown in figure 1(*b*).

## 3. Experimental procedure and analysis

To measure thermal conductivity of the freestanding nitride specimens, we pass dc current through the aluminum heaters. Since the heater line is also freestanding, the Joule heating develops a parabolic temperature profile with the highest temperature in the middle section, which intersects the silicon nitride specimen and supplies a heat flux to it. In a typical experiment, 4–10 milliamps of current is passed to raise the middle section of the heater (and the silicon nitride) from 310 to 375 K. The temperature distribution along the length of the heater is measured using an infrared microscope (Quantum Focus Instruments, MWIR-512 InSb IR FPA camera) with 0.1 K temperature and 2 $\mu$m spatial resolution. The inset in figure 1(*b*) shows a thermal micrograph of the heater during operation. At the same time, the temperature profile along the length of the silicon nitride specimen is measured. Calculation of the thermal conductivity requires the heat flux in the specimen, which can be approximated from the power supply to the heater, or more accurately by performing finite element simulation [35]. We used commercially available software COMSOL Multiphysics$^{TM}$ to carry out the finite element solution of the described problem. Among the various application modes, electro-thermal application mode is used for the modeling as this problem incorporates Joule heating of the material. This mode presents the coupling of three different basic application modes which are conductive media dc application, heat transfer application and solid mechanics application modes. Heat loss through convection and conduction (through the air to the etched substrate below the specimen) was included in the model. Tables 1 and 2 describe primary input parameters for the model. The physical properties [37] are taken for bulk scale since silicon nitride is

**Table 1.** Multi-physics modules and input parameters.

| Application mode | Properties | Silicon nitride | Aluminum |
|---|---|---|---|
| Conductive media dc mode | Resistivity (Ω m) | 1.72e12 | 3.75e-8 |
| | Temperature coefficient of resistance (1/K) | 0.0038 | 0.003 |
| | Reference temp (K) | 300 | 300 |
| Heat transfer mode | Thermal conductivity (W (m K)$^{-1}$) | Varied to match measured temperature profile | 237 |
| | Density (kg m$^{-3}$) | 3100 | 2700 |
| | Heat capacity, $C_p$ (J (kg K)$^{-1}$) | 700 | 904 |
| Solid mechanics mode | Young's modulus (Pa) | 250e9 | 70e9 |
| | Poisson's ratio | 0.23 | 0.35 |
| | Thermal expansion coefficient (1/K) | 2.3e-6 | 23.1e-6 |
| | Density (kg m$^{-3}$) | 3100 | 2700 |

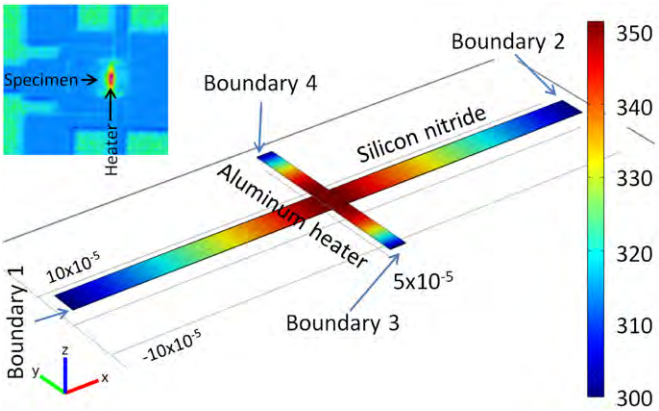


**Figure 3.** Multi-physics simulation model for the device showing temperature profile at zero strain. Infrared microscopy shows the large drop in thermal conductivity at 2.4% strain (inset).

**Table 2.** Geometry parameters for the aluminum and silicon nitride structures.

| Material | Length ($\mu$m) | Width ($\mu$m) | Thickness ($\mu$m) |
|---|---|---|---|
| Aluminum | 35 | 3 | 0.175 |
| Silicon nitride | 100 | 5 | 0.050 |

an amorphous material and aluminum film is too thick to show any size effect.

Figure 3 shows the finite element model, where the four boundaries are numbered for the ease of identification. The conductive media dc mode solves the following equation:

$$-\nabla \cdot (\sigma \nabla V - J^e) = Q_j, \tag{6}$$

where $\sigma$ is the electrical conductivity, $V$ is the potential, $J^e$ is the external current density and $Q_j$ is the current source. This mode assumes that the model has symmetry and the electric potential varies only in the $X$ and $Y$ directions and is constant in the $Z$ (film thickness) direction. For Joule heating, the electrical conductivity is temperature dependent and maintains the following relationship:

$$\sigma = \frac{1}{\rho_o(1 + \alpha(T - T_o))}, \tag{7}$$

where $\rho_o$ is the resistivity at reference temperature $T_0$ and $\alpha$ is the temperature coefficient of resistance. One end of the aluminum heater (boundary 3) is provided with an electric potential ($V = V_o$) and the opposite end (boundary 4) is electrically grounded, as shown in figure 4. All other boundaries of aluminum and silicon nitride are chosen to be electrically insulated ($n.J = 0$).

The heat transfer mode solves the following governing equation:

$$\nabla(-k\nabla T) = Q + q_s T, \tag{8}$$

where $k$ is the thermal conductivity, $\nabla T$ is the temperature gradient, $Q$ is the heat generation and $q_s$ is the production/absorption coefficient. The four ends of the aluminum and silicon nitride films (boundaries 1, 2, 3 and 4) are kept at constant temperature ($T = T_0$). This is because the thermal mass of the substrate is enormous compared to the aluminum and nitride films. For all other boundaries, heat flux boundary condition is applied through the following equation:

$$-n.q = q_o + h(T_0 - T), \tag{9}$$

where $n$ is the outward normal, $q$ is the conductive heat flux vector, $q_o$ is the inward heat flux from external sources (such as radiation) and $h$ is the convection heat transfer coefficient. In this study $T_0$ is taken to be 300 K. Because the experiments were conducted at lower temperatures, radiation was neglected. At the same time, heat loss through air (in this case, from the bottom surface of the nitride specimen to the device floor) is known to be dominant in the literature [38], which was incorporated through an 'effective convective heat transfer coefficient'. A sensitivity analysis of the multi-physics model yielded the value of $h_{\text{air}} = 500$ W m$^{-2}$ K$^{-1}$ for the etch depth of about 15 $\mu$m in our study, for which the temperature profiles in the specimen and the heater were in very close agreement for all input current values. A simple scaling analysis may suggest higher values ($h_{\text{air}} = 1666$ W m$^{-2}$ K$^{-1}$), but is unable to reproduce the actual temperature profile in the specimen.

The solid mechanics mode employs the governing equation

$$\sigma = E\varepsilon, \tag{10}$$

where $\sigma$ is the stress, $E$ is Young's modulus and $\varepsilon$ is the net strain. The net strain includes applied elastic strain, thermal strain and initial strain. Boundaries 1, 2, 3 and 4 are constrained with fixed boundary condition (displacement is zero in all directions), while all other boundaries are considered as constraint free. No external load is applied to the boundaries.

To validate the model, we compare the simulated temperature profile along the aluminum heater line with that obtained from simulation for different values of input current. Figure 4 shows the excellent agreement between the actual and simulated heater temperature profiles. It also shows the heat flux value from the simulation. Since the governing equations of the finite element model do not have any strain–thermal conductivity coupling, we first measure the temperature profile along the specimen length for various levels of mechanical strain. To extract the thermal conductivity of the specimen for each strain values, we simulate the heat flow for the calculated heat flux values for various trial values of thermal conductivity until the simulated temperature profile closely matched that obtained from thermal microscopy. Figure 5 shows this procedure for two different values of strain.

## 4. Results and discussion

Figure 6 shows the experimental results for room temperature thermal conductivity of 50 nm thick freestanding amorphous silicon nitride as a function of mechanical strain up to 2.4%. The fracture strain of silicon nitride can be as high as 3% [39, 40]. Also shown (in latter form) are the data taken from the literature for comparable specimen thicknesses. The literature data are shown at about 0.3% strain because even though the specimens are freestanding, their clamped edge boundary conditions do not relieve the residual strain. These studies involve $SiN_x$ (also known as low stress or hydrogen rich silicon

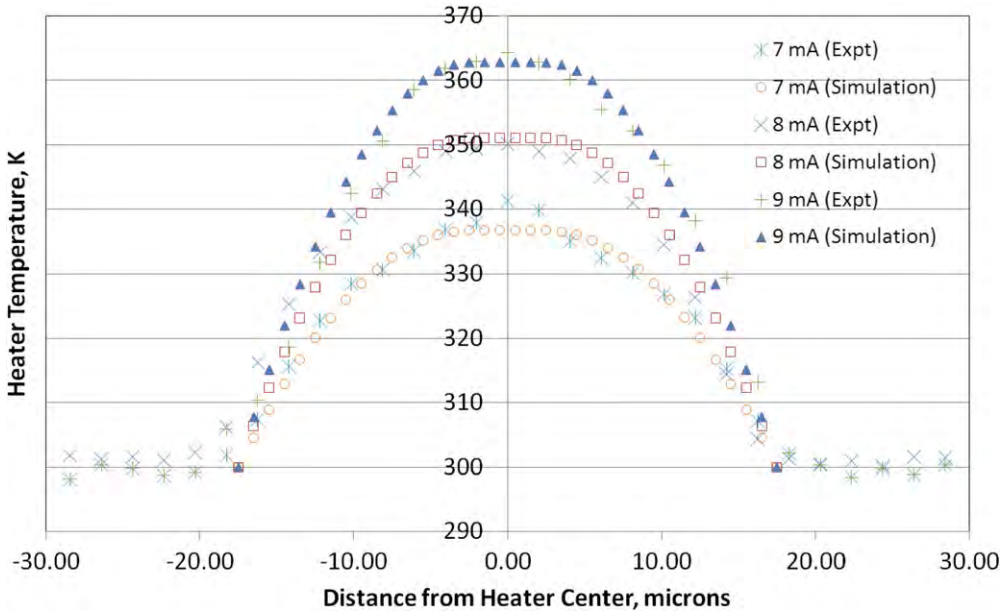


**Figure 4.** Comparison of the experimental and simulation results on the heater temperature profile as a function of input current.

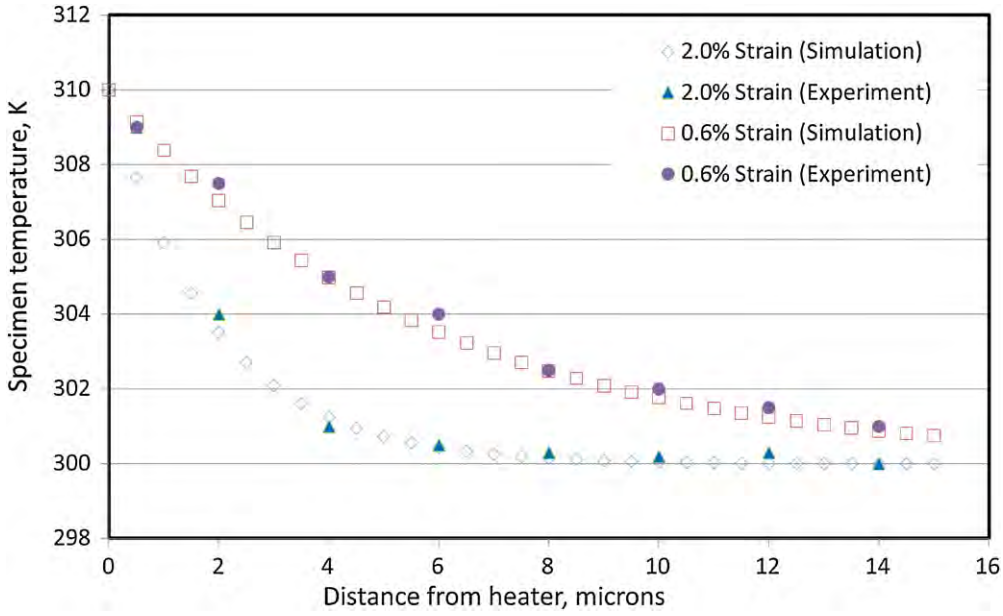


**Figure 5.** Comparison of experimental and simulation results on the temperature profile of the silicon nitride specimens with fitted values of thermal conductivity.

nitride) with $x$ varying from 1 to 1.1, for which the residual strain reported is about 0.2%–0.3% [41]. When interpolated between 0% and 0.6% strain, our results are in excellent agreement with the literature except for two instances (studies D and E). These two studies involved specimens on substrate, for which thermal conductivity is expected to show a pseudo-size effect unless corrected for thermal contact resistance. This is because such cross-plane measurements involve nanoscale length of heat flow path ($L$ = specimen thickness) and two interfacial thermal resistances ($\rho_{\text{th}}$) [42]

$$\frac{1}{\kappa(T,L)} = \frac{1}{\kappa(T,L\to\infty)} + \frac{A\rho_{\text{th}}}{L}, \tag{11}$$

where $A$ is the cross-section of the specimen. Lee and Cahill [33] explained their observed size effect with the above argument, while Bai *et al* [36] corrected their data after developing a technique to measure the interfacial thermal resistance.

Two concerns related to the experimental technique deserve further scrutiny. The first one is on the role of interfacial thermal resistance, which is typically not critical for in-plane thermal conductivity measurements. This is verified by plugging in representative values from our experiments in equation (11). For the heater–specimen interfacial area $A = 25\times10^{-12}$ m$^2$, $\rho_{\text{th}}$= 2–3 $\times 10^{-8}$ m$^2$K W$^{-1}$[33, 36] and $L$ is about $15\times10^{-6}$ m), the size dependent term is

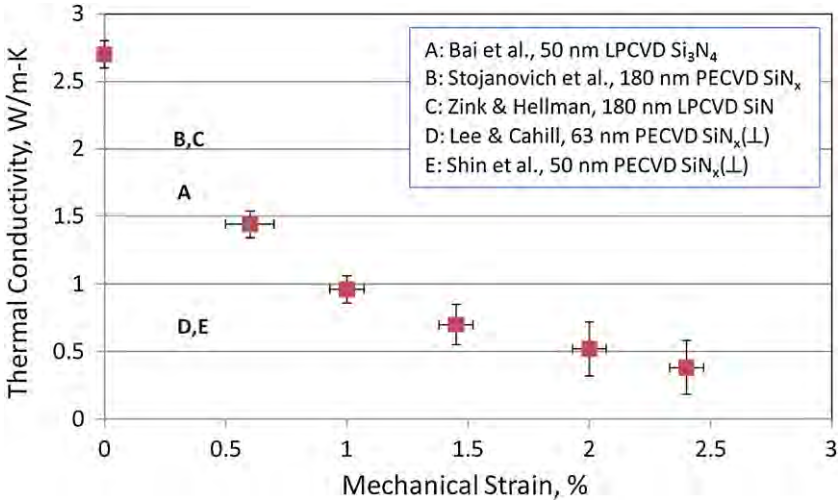


**Figure 6.** Thermal conductivity of 50 nm thick $Si_3N_4$ films as a function of mechanical strain. The letters corresponding to 0.3% strain represent data from the literature. The symbol (⊥) denotes cross-plane thermal conductivity data.

only about $6.25 \times 10^{-14}$, which clearly shows that interfacial thermal resistance is not a critical concern for this study. The second concern arises from the amount of strain developed in the aluminum heater due to the strain in the silicon nitride specimen, which may change the electrical and thermal properties of the heater and introduce experimental errors. For a 125 nm thick aluminum film on silicon oxide, such strain effects have been shown to be pronounced [27], which calls for a detailed analysis. Since the freestanding aluminum heater is attached to the nitride specimen at the midpoint, the maximum strain it experiences is the same as the net strain in the width direction of the nitride specimen. This is given by

$$\varepsilon_{Al} = \varepsilon_y = \frac{(-\nu\sigma_x + \sigma_y)}{E} + \varepsilon_{\text{residual}}, \tag{12}$$

where $x$ and $y$ directions are along the length and width of the silicon nitride specimen, respectively, and Poisson's ratio $\nu = 0.22$. The residual strain is about 0.4% for our specimens and is bi-axial and tensile in nature. The actuation method applies uni-axial tension in the nitride specimens with stress ($\sigma_x$) about 6 GPa for about 2.4% strain (the fracture stress of silicon nitride varies from 8 to 10 GPa). For these values, the net strain in the aluminum heater considering the Poisson effect is −0.5%. In other words, there is no appreciable strain developed in the aluminum heater for the actuated nitride specimens. This is also verified by our measurements of electrical resistance of the aluminum heater before and after the release from substrate, which did not show any appreciable change in the resistance due to the loading of the heater line. For zero strain–thermal conductivity measurements, the tensile strain in the heater segment overlapping the nitride specimen is about 0.4%, for which the thermal conductivity was assumed to be 100 W (m K)$^{-1}$ [27].

To explain the observed influence of strain on thermal conductivity, we note that commonly cited size effects for low-dimensional materials [23, 43] and hetero structures [44, 45] cannot be used because of the amorphous microstructure of the specimens. The phonon mean free path of amorphous materials is of the same order as the structural disorder [46], rendering thermal conductivity size independent. Here, the phases of the atomic vibrations are incoherent and the oscillators are damped strongly enough to pass their energy to the neighbors within half the period of oscillation; yet the states are not localized. In other words, heat transfer in amorphous solids is a random walk of energy between localized oscillators of varying sizes and frequencies. The Cahill and Pohl [47] model for thermal conductivity of amorphous materials integrates the specific heat ($C$), phonon velocity ($v$) and the mean free path ($l$) over the entire range of frequencies

$$k_{\text{diff}} = \frac{1}{3}\int_0^\infty \frac{\mathrm{d}C}{\mathrm{d}\omega} v(\omega) l(\omega)\, \mathrm{d}\omega. \tag{13}$$

In real amorphous materials, the inherent aperiodicity gives rise to strong localization of high frequency vibrations or 'fractons'. Orbach and co-workers therefore suggested an alternative mode of heat transfer, modeled by hopping energy through highly localized vibrational modes (fractons) that are coupled to phonons via the anharmonic interaction [48]. While fractons alone in a harmonic system cannot transfer heat, it has been shown in the literature that anharmonicity induces interaction between phonons and fractons that allow transfer of energy from a localized excitation to other. Such fraction–phonon interaction resembles spatial overlapping of the localized vibrational modes [49]. Without such overlap, amorphous materials would exhibit zero thermal conductivity. At the same time, the overlap must be minimal because amorphous materials are known to exhibit very low thermal conductivity. Therefore, we propose that overlap is extremely marginal and sensitive to tensile deformation. This is supported by our experimental observation of about one order of magnitude reduction in thermal conductivity at about 2.4% strain. On the other hand, compressive deformation would only increase such overlap, which will eliminate the influence of strain, unless the stress is so large that the elastic constants are changed. Interestingly, this conjecture is supported by both theory and recent experiments [26].

While the influence of strain on thermal conductivity is not a size effect, we suggest that it depends on the vibrational

density of states, which in turn depends on atomic bond energy, distance etc parameters. Unlike crystalline materials, where all the modes are non-localized (diffusive), amorphous materials show the spectra of both localized (fraction) and diffusive (phonon) modes [50]. Therefore, the thermal conductivity can be expressed as

$$k(T) = k_{\text{diff}}(T) + k_{\text{hop}}(T). \quad (14)$$

Our conceptual model suggests that the strain–thermal conductivity coupling would depend on the relative contribution of these two modes, which in turn, depend on the lack of long-range order and atomic bond energy. Crystalline or polycrystalline materials exemplify diffusion-dominated thermal transport, for which very large strain (∼10% [23]) or stress (∼20 GPa [51]) is shown to produce only modest reduction in thermal conductivity at the extremely small (<10 nm) length scales. The lack of long-range order in amorphous materials gives rise to the predominance of fractons in the vibrational density of states. For example, the sharpest peak for amorphous silicon is at the frequency of 66 meV, which is very close to the cutoff (below which the localization effect is too strong to transport heat) value of 72 meV [52]. We hypothesize that the relative contribution of fractons in thermal transport of amorphous materials is dependent on the bond energy of the atoms. While the vibrational density of states of silicon nitride is not available in the literature, we expect the peak frequency to be higher than amorphous silicon because the Si–N bond energy (78.32 kcal/mol) is much higher than the Si–Si bond (53.31 kcal/mol) [53]. Amorphous silicon nitride is therefore expected to show stronger vibration localization compared to amorphous silicon. This implies that strain–thermal conductivity coupling in amorphous solids will also depend on the bond type and energy. Currently, we are performing atomistic simulations to verify this hypothesis.

## 5. Conclusion

In this study, we investigated the concept of tuning thermal conductivity of nanoscale solids using externally applied mechanical strain. We developed an experimental technique to apply controllable strain on freestanding amorphous silicon nitride specimens and measure their thermal conductivity. We demonstrate the technique on 50 nm thick specimens at up to 2.4% strain. It is commonly held that amorphous solids already show minimum values of thermal conductivity strain at zero strain and hence are expected to show the weakest strain–transport coupling. In contrast, our experimental results show very strong influence on thermal conductivity, which decreased from 2.7 to 0.34 W (m K)$^{-1}$ under 2.4% strain. We propose that thermal conductivity in amorphous solids is a strong function of vibration localization, which increases with tensile strain. We conclude that crystalline solids do not show such strong coupling because of their non-localized vibrational modes.

## Acknowledgments

MAH gratefully acknowledges the support from the Center for Nanoscale Mechatronics and Manufacturing of the Korea Institute of Machinery and Materials, the National Science Foundation, USA (ECCS 1028521) and the United Technology Corporation (sub-contract: 10-S587-031-01-C6). The authors acknowledge in-depth discussion with Sergei Shenogin of the Air Force Research Laboratory.

## References

[1] DeVoe D L 2002 Thermal issues in MEMS and microscale systems *IEEE Trans. Compon. Packag. Technol.* **25** 576–83
[2] Mahajan R, Chiu C P and Chrysler G 2006 Cooling a microprocessor chip *Proc. IEEE* **94** 1476–86
[3] Long J *et al* 2008 Thermal monitoring mechanisms for chip multiprocessors *ACM Trans. Archit. Code Optim.* **5** (2) 1–33
[4] Gadag S P *et al* 2002 Design and analysis: thermal emulator cubes for opto-electronic stacked processor *J. Electron. Packag.* **124** 198–204
[5] Lin S, Sefiane K and Christy J R E 2002 Prospects of confined flow boiling in thermal management of microsystems *Appl. Therm. Eng.* **22** 825–37
[6] Choi S H *et al* 2008 The effect of electrode heat sink in organic-electronic devices *Appl. Phys. Lett.* **93** 183301
[7] Feng J and Ellis T W 2003 Thermal management for semiconductor devices with conductive polymers *Synth. Met.* **135** 155–6
[8] Chen G *et al* 2003 Recent developments in thermoelectric materials *Int. Mater. Rev.* **48** 45–66
[9] Li S *et al* 2003 Measuring thermal and thermoelectric properties of one-dimensional nanostructures using a microfabricated device *J. Heat Transfer* **125** 881–8
[10] Miner A and Ghoshal U 2006 Limits of heat removal in microelectronic systems *IEEE Trans. Compon. Packag. Technol.* **29** 743–9
[11] Haque M A and Saif M T A 2005 Thermo-mechanical properties of nano-scale freestanding aluminum films *Thin Solid Films* **484** 364–8
[12] Olliges S *et al* 2011 Thermo mechanical properties and plastic deformation of gold nanolines and gold thin films *Mater. Sci. Eng.* A **528** 6203–9
[13] Shen Y L 2006 Thermo-mechanical stresses in copper interconnects—a modeling analysis *Microelectron. Eng.* **83** 446–59
[14] Maeda M and Nakamura H 1984 Insulation degradation and anomalous etching phenomena in silicon nitride films prepared by plasma-enhanced deposition *Thin Solid Films* **112** 279–88
[15] Eriksson P, Andersson J Y and Stemme G 1997 Thermal characterization of surface-micromachined silicon nitride membranes for thermal infrared detectors *J. Microelectromech. Syst.* **6** 55–61
[16] Manninen A J, Leivo M M and Pekola J P 1997 Refrigeration of a dielectric membrane by superconductor/insulator/normal-metal/insulator/superconductor tunneling *Appl. Phys. Lett.* **70** 1885–7
[17] Olson E A *et al* 2003 The design and operation of a MEMS differential scanning nanocalorimeter for high-speed heat capacity measurements of ultrathin films *J. Microelectromech. Syst.* **12** 355–64
[18] Lin C-H *et al* 2005 Effect of strain on *p*-channel metal-oxide-semiconductor field-effect-transistor current enhancement using stress-modulated silicon nitride films *Appl. Phys. Lett.* **87** 262109
[19] Liang-Teck P *et al* 2009 Measurement and analysis of variability in 45 nm strained-Si CMOS technology *IEEE J. Solid-State Circuits* **44** 2233–43
[20] Picu R C, Borca-Tasciuc T and Pavel M C 2003 Strain and size effects on heat transport in nanostructures *J. Appl. Phys.* **93** 3535–9

[21] Bhowmick S and Shenoy V B 2006 Effect of strain on the thermal conductivity of solids *J. Chem. Phys.* **125** 164513
[22] Linli Z and Xiaojing Z 2009 Modification of the phonon thermal conductivity in spatially confined semiconductor nanofilms under stress fields *Europhys. Lett.* **88** 36003
[23] Li X *et al* 2010 Strain effects on the thermal conductivity of nanostructures *Phys. Rev.* B **81** 245318
[24] Kulkarni A J and Zhou M 2007 Tunable thermal response of ZnO nanowires *Nanotechnology* **18** 435706
[25] Shen S *et al* 2010 Polyethylene nanofibres with very high thermal conductivities *Nature Nanotechnol.* **5** 251–5
[26] Hsieh W-P *et al* 2011 Testing the minimum thermal conductivity model for amorphous polymers using high pressure *Phys. Rev.* B **83** 174205
[27] Lee H F, Kumar S and Haque M A 2010 Role of mechanical strain on thermal conductivity of nanoscale aluminum films *Acta Mater.* **58** 6619–27
[28] Mastrangelo C H, Tai Y-C and Muller R S 1990 Thermophysical properties of low-residual stress, silicon-rich, LPCVD silicon nitride films *Sensors Actuators* A **23** 856–60
[29] Zhang X and Grigoropoulos C P 1995 Thermal conductivity and diffusivity of free-standing silicon nitride thin films *Rev. Sci. Instrum.* **66** 1115–20
[30] Jain A and Goodson K E 2008 Measurement of the thermal conductivity and heat capacity of freestanding shape memory thin films using the 3 omega method *J. Heat Transfer* **130** 102402
[31] Sultan R *et al* 2009 Thermal conductivity of micromachined low-stress silicon-nitride beams from 77 to 325 K *J. Appl. Phys.* **105** 043501
[32] Zink B L and Hellman F 2004 Specific heat and thermal conductivity of low-stress amorphous Si–N membranes *Solid State Commun.* **129** 199–204
[33] Lee S M and Cahill D G 1997 Heat transport in thin dielectric films *J. Appl. Phys.* **81** 2590–5
[34] Shin S W, Cho H N and Cho H H 2006 Measurement of thermal conductivity of silicon nitride thin films *Int. Heat Transfer Conf. 13* ed G de Vahl Davis and E Leonardi (Sydney: Begell House) THP-05
[35] Stojanovic N *et al* 2007 Thin-film thermal conductivity measurement using microelectrothermal test structures and finite-element-model-based data analysis *J. Microelectromech. Syst.* **16** 1269–75
[36] Bai S *et al* 2009 Thermal characterization of $Si_3N_4$ thin films using transient thermoreflectance technique *IEEE Trans. Indust. Electron.* **56** 3238–43
[37] Shackelford J F, Alexander W and Park J S 1994 *CRC Materials Science and Engineering Handbook* (Boca Raton, FL: CRC Press)
[38] Hu X J, Jain A and Goodson K E 2008 Investigation of the natural convection boundary condition in microfabricated structures *Int. J. Therm. Sci.* **47** 820–4
[39] Kaushik A, Kahn H and Heuer A H 2005 Wafer-level mechanical characterization of silicon nitride MEMS *J. Microelectromech. Syst.* **14** 359–67
[40] Wen-Hsien C *et al* 2004 Mechanical property characterization of LPCVD silicon nitride thin films at cryogenic temperatures *J. Microelectromech. Syst.* **13** 870–9
[41] French P J *et al* 1997 Optimization of a low-stress silicon nitride process for surface-micromachining applications *Sensors Actuators* A **58** 149–57
[42] Poetzsch R H and Bottger H 1994 Interplay of disorder and anharmonicity in heat conduction: molecular-dynamics study *Phys. Rev.* B **50** 15757–63
[43] Ballandin A and Wang K L 1998 Significant decrease of the lattice thermal conductivity due to phonon confinement in a free-standing semiconductor quantum well *Phys. Rev.* B **58** 1544–9
[44] Vikas S and Vikas T 2010 The role of straining and morphology in thermal conductivity of a set of Si–Ge superlattices and biomimetic Si–Ge nanocomposites *J. Phys. D: Appl. Phys.* **43** 135401
[45] Xu Y and Li G 2009 Strain effect analysis on phonon thermal conductivity of two-dimensional nanocomposites *J. Appl. Phys.* **106** 114302
[46] Freeman J J and Anderson A C 1986 Thermal conductivity of amorphous solids *Phys. Rev.* B **34** 5684–90
[47] Cahill D G and Pohl R O 1988 Lattice vibrations and heat transport in crystals and glasses *Annu. Rev. Phys. Chem.* **39** 93–121
[48] Jagannathan A, Orbach R and Entin-Wohlman O 1989 Thermal conductivity of amorphous materials above the plateau *Phys. Rev.* B **39** 13465
[49] Leitner D M 2001 Vibrational energy transfer and heat conduction in a one-dimensional glass *Phys. Rev.* B **64** 094201
[50] McGaughey A J H and Kaviany M 2006 Phonon transport in molecular dynamics simulations: formulation and thermal conductivity prediction *Advances in Heat Transfer* ed G A Greene, J P Hartnett and A Bar-Cohen *et al* (Amsterdam: Elsevier) pp 169–255
[51] Zhu L and Zheng X 2009 Modification of the phonon thermal conductivity in spatially confined semiconductor nanofilms under stress fields *Europhys. Lett.* **88** 360003
[52] Allen P B *et al* 1999 Diffusons, locons and propagons: character of atomic vibrations in amorphous Si *Phil. Mag.* B **79** 1715–31
[53] Leroy G *et al* 1992 Determination of bond energy terms in silicon-containing compounds *J. Mol. Struct.: THEOCHEM* **259** 369–81